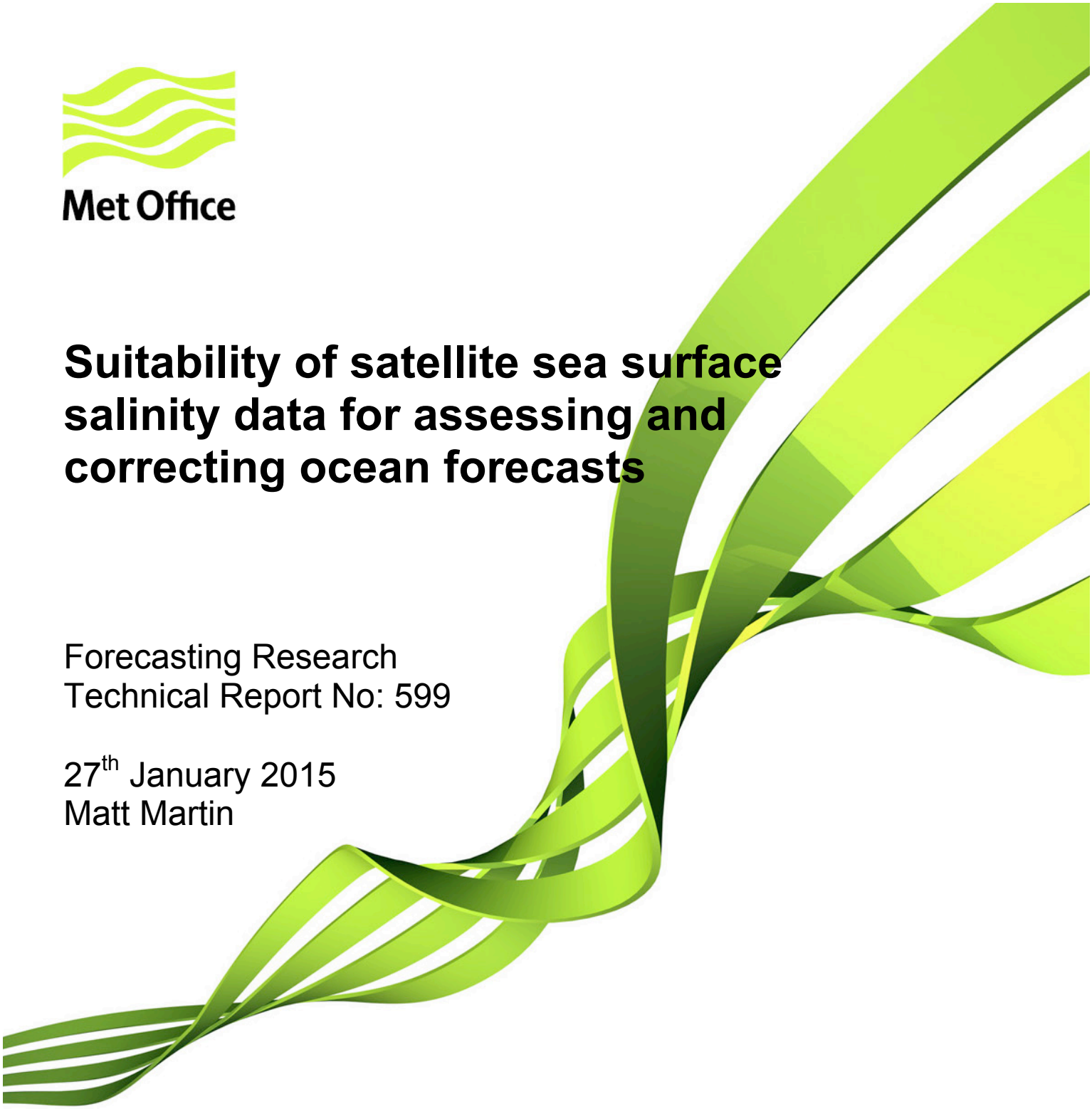

Suitability of satellite sea surface salinity data for assessing and correcting ocean forecasts

Forecasting Research
Technical Report No: 599

27th January 2015
Matt Martin

Contents

Summary **3**

1. Introduction **3**

2. Data sources **5**

2.1 In situ data 5

2.2 SMOS data 5

2.3 Aquarius data 5

2.4 FOAM data 6

3. Comparison methodology **7**

4. Assessment of satellite surface salinity data **7**

4.1 FOAM vs Argo 8

4.2 Which SMOS product to use? 9

4.2.1. Ascending vs descending SMOS data 10

4.2.2. RFI flags in SMOS data 10

4.2.3. Temporal averaging 10

4.2.4. Spatial averaging 13

4.3 Comparison of SMOS and Aquarius 15

5. Spatial information in SMOS **16**

6. Conclusions and discussion **20**

Acknowledgements **21**

© Crown copyright 2015

Summary

Sea surface salinity (SSS) data from the Forecasting Ocean Assimilation Model (FOAM) system are used to understand various characteristics of satellite SSS data from the SMOS and Aquarius missions. The errors in the model fields are first estimated by comparing them to near-surface Argo salinity measurements, with RMS errors of less than 0.2 pss and regional biases of less than 0.05 pss. Various processing versions of the SMOS data are assessed, including different temporal and spatial averaging, and the daily 1° resolution SMOS and Aquarius differences to FOAM are roughly 3-10 times larger than Argo-FOAM differences. The spatial information in the SMOS data is also assessed by comparing spatial gradients in the satellite SSS data with those calculated from other datasets including satellite SST and satellite altimeter SSH data, as well as with the model's gradients. The SMOS data contains information about the underlying ocean dynamics in the summer months which are not present in the satellite SST data or in the model's SSS fields. This demonstrates that the data contains useful information which could be used to correct the model through data assimilation.

1. Introduction

Ocean forecasting systems such as the Forecasting Ocean Assimilation Model (FOAM) system (Blockley *et al.*, 2014) aim to produce accurate forecasts of the three-dimensional ocean temperature, salinity and currents, as well as sea-ice variables, for various users including the Royal Navy, search and rescue, oil spill, ship routing, oil and gas, and research users. This system is also now being used in conjunction with the existing Met Office Numerical Weather Prediction (NWP) system to develop short- to medium-range coupled ocean/atmosphere forecasts. For both forced-ocean and coupled ocean/atmosphere forecasting, understanding the errors at the sea surface provides an important method for identifying sources of forecast error, as the impact of the atmospheric forcing on the ocean is then directly observable. We can then more easily distinguish the sources of errors between atmospheric forcing and internal ocean model errors which is difficult if only sparse sub-surface observations are available.

Assessment of surface temperature errors has taken place routinely for many years due to the large amount of sea surface temperature (SST) data available, for example through the Group for High Resolution SST (Donlon *et al.*, 2010). The other variable affecting the ocean's density, salinity, has not been observed to anywhere near the same extent as temperature. Argo provides a very useful data-set of salinity since about 2003 (Freeland *et al.*, 2010), but the data are sparse (roughly 3°x3° horizontal resolution every 10 days) and usually only measure within about 5 m of the surface. The relatively new data-sets provided by the Soil Moisture Ocean Salinity (SMOS; Font *et al.*, 2012) and Aquarius (Lagerloef *et al.*, 2012) satellite missions, launched in 2009 and 2011 respectively, provide a wealth of sea surface salinity (SSS) information which could be exploited through model assessment and assimilation.

SSS is a difficult quantity to measure from space for various reasons. The brightness temperatures measured by satellites in the L-band are related to the SSS through a complicated relationship which includes dependence on SST as well as the sea surface roughness induced by waves and foam (Yin *et al.*, 2012a), Galactic radiation

© Crown copyright 2015

at L-band frequencies are reflected by the sea surface and can contaminate the signal received by the satellites with varying power depending on the time of day (Le Vine and Abraham, 2004). The reflection of solar radiation by the sea surface also affects the signal received by the satellite in the L-band and this sun glint needs to be accounted for (Reul *et al.*, 2007). Radio frequency interference (RFI) from sources over land also has significant impacts on the retrieved salinity (Oliva *et al.*, 2012). Calibration and validation of the retrieved surface salinity is also challenging given the different depth sampling and sparse horizontal sampling of the in situ salinity network, as described in Tang *et al.* (2014).

Despite all these complications in the retrieval of SSS from space, numerous investigations have demonstrated that important ocean processes can be seen in satellite SSS data. Lee *et al.* (2012) show that Aquarius data can detect Tropical Instability Waves (TIWs) in the Pacific; Yin *et al.* (2014) demonstrate that SMOS also detects TIWs. Grodsky *et al.* (2012) show the impact of hurricanes on surface salinities in the Amazon/Orinoco river plume and the important relationships between surface salinity and the mixing of heat associated with a hurricane. Gierach *et al.* (2013) use Aquarius and SMOS data to detect a river flooding event in the Gulf of Mexico. Boutin *et al.* (2013) investigate the relationship between rain rates and surface ocean freshening in satellite observations. Reul *et al.* (2014) demonstrate the ability of SMOS data to identify mesoscale structures in the Gulf Stream which are not well-observed by SST data in the summer months, and which correspond to features measured by sea level satellite data.

A few studies to date have investigated the suitability of SMOS and Aquarius data to be used for ocean model assessment and assimilation. Vinogradova *et al.* (2014) carry out a model-data comparison exercise for both SMOS/Aquarius satellite and in situ surface salinity measurements to understand the relative errors in each estimate, with the aim of using those error estimates in future assimilation studies. The model used is in that study is part of the ECCO system (Wunsch and Heimbach, 2013), with the model data coming from a model-only (no data assimilation) run of the MITgcm and comparisons carried out for the period September 2011 to December 2012. Köhl *et al.* (2014) assimilate SMOS data into the GECCO2 system. They find that the assimilation of SMOS data only has a significant impact if the observation errors specified in the assimilation system are artificially reduced by an order of magnitude. The impact of the data, once the specified errors are reduced, is to reverse the sign of the surface salinity bias in the analysis (assessed using in situ salinity measurements), compared to a run which did not assimilate the SMOS data.

This work follows a similar approach to that of Vinogradova *et al.* (2014) in order to understand the errors in the satellite SSS data. Instead of the ECCO system, which is used for climate studies and assimilates data using an adjoint approach, we use the FOAM system which is an operational ocean forecasting system and which assimilates data using a 3DVar methodology. Rather than the monthly fields assessed in that study we look at higher temporal resolution data (model and observation); the model data here comes from an assimilative run rather than the model-only integration used in that study; and the SMOS data used here is a Level 3 product rather than the objective analysis used in that study; they do not estimate biases. More detail on the FOAM system and the specific model data used in this study is provided in section 2, as well as information on the SMOS, Aquarius and in situ data-sets used. The techniques used to compare the model and observational data are described in section 3. The results of those comparisons are presented in section 4, including a comparison of the FOAM SSS forecasts with Argo data, comparisons with various SMOS products, and with Aquarius data. Section 5 examines the horizontal gradients present in the model and satellite observational

© Crown copyright 2015

data-sets in order to illustrate the information available on spatial structures in particular regions. Section 6 discusses the results and provides some conclusions.

2. Data sources

2.1 In situ data

Argo profiling floats measure temperature and salinity over the top 2000m of the ocean with a resolution of roughly 3°x3° every 10 days. The salinity is measured to an accuracy of approximately ± .01 pss, but the salinity sensors can be affected by drifts which are usually corrected for in delayed mode. Due to the likelihood of fouling of the sensors, the pump which moves the water over the salinity sensor is switched off usually at 4m depth and so only a few salinity measurements are available closer to the surface than this. A consistently quality controlled data-set, EN3 (Ingleby and Huddleston, 2007), is used as the source of the Argo data in this study. Only data in the top 10m depth of the ocean are used, with values representing an average over that depth. Fig 1a shows the coverage of Argo salinity measurements for one day (1st Feb 2012), illustrating the sparse coverage from the in situ data.

2.2 SMOS data

A number of institutes produce level 3 (gridded but not interpolated) processed SMOS products. The data used in this study are taken from the expertise centres of CATDS (http://www.catds.fr/Products/Available-products-from-CEC-OS) which contains two data-sets: one processed by Ifremer and one by LOCEAN (Yin *et al.*, 2012b). LOCEAN maps are based on the level 2 data processing of ESA while the IFREMER product uses slightly different algorithms and flags. In particular the Ifremer processing includes the use of climatological salinity in order to improve the data sorting in areas affected by RFI, and correct for systematic biases near land and at high latitudes. Data-sets from both institutes are produced at 0.25, 0.5 and 1° horizontal resolutions, with daily, 10-day and monthly products available. LOCEAN data comes with mean theoretical error estimates of the SSS measurements used to derive the mean SSS at the pixel level which are not available in the Ifremer product. Conversely, the Ifremer product contains information about the likely probability of each data point being contaminated by RFI. Fig 1b shows the coverage of SMOS L3 data available for one day (1st Feb 2012) from the Ifremer 1° resolution daily product. The impact of RFI is clearly visible, for example in the reduced number of observations in the Bay of Bengal.

2.3 Aquarius data

The Aquarius data used in this study was obtained from the Jet Propulsion Laboratory's (JPL) Physical Oceanography Distributed Active Archive Center (PO.DAAC). Version 2.0 of the level 3 gridded data is used at 1° horizontal resolution and daily temporal resolution. Fig 1c shows the number of Aquarius L3 data available for one day (1st Feb 2012).There are generally fewer Aquarius observations than for the equivalent SMOS data due to the width of the swath, but there are more data near to the coasts, particularly in the north Indian Ocean and western north Pacific.

© Crown copyright 2015

2.4 FOAM data

The FOAM data used here is from the "v13" experiment described in Blockley *et al.* (2014) which is a recent integration of the global FOAM system at ¼° horizontal resolution. The vertical resolution of the model is roughly 1m in the top ten metres, with 75 vertical levels in total. The model is the Nucleus for European Modelling of the Ocean (NEMO) code (Madec, 2008) which is coupled to the CICE sea-ice model (Hunke and Lipscomb, 2010), and the integration includes assimilation of data using the NEMOVAR scheme (Waters *et al*., 2014). The assimilated data include satellite and in situ SST, satellite altimeter sea level anomaly (SLA), satellite sea-ice concentration data, and in situ profiles of temperature and salinity from various sources including Argo, moored buoys, XBTs, gliders and marine mammals. Due to the lack of SSS data available for assimilation, the model's surface salinity forecast is relaxed towards climatological estimates by adjusting the surface freshwater flux with a damping time-scale of 33.33 mm/day/pss. Daily mean model fields are used in this study with the top model level being used, representing an average over the top 1m of the ocean.

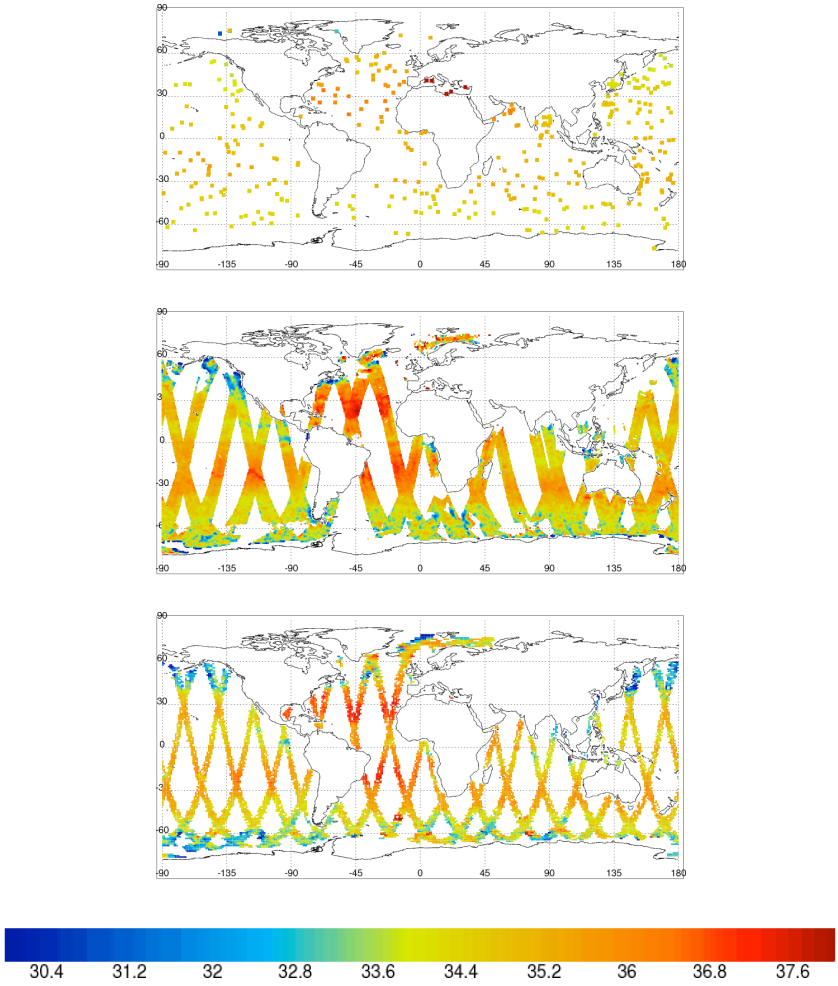

Fig 1. Example observation coverage for one day (1st Feb 2012) for (a) Argo, (b) SMOS (1°, daily product from Ifremer) and (c) Aquarius (1°, daily product from PO.DAAC). The values are sea surface salinity (pss).

© Crown copyright 2015

3. Comparison methodology

When comparing model data with observations it is important to compute the equivalent model value of the observations accurately so that the two estimates represent the same spatial and temporal scales. In the results which follow, the gridded model values are bilinearly interpolated to the location of the Argo observations when comparing model and in situ data. In order to compute the model equivalent of the satellite SSS data, we have produced weighted averages of the model data with the same footprint as the observations. For the observation products in which the observational data are temporally averaged over more than one day, the model data has also been temporally averaged over the same periods. For the Argo data (which is valid at a particular time of day) the model data at the nearest model time-step (20 minutes) is used. Using these methods, the model equivalents of the various observational data-sets have been produced for the period 1st December 2011 to 30th November 2012.

The triple collocation technique used in Stoffelen (1998) and Vinogradova *et al.* (2014) could be used here to assess the relative accuracy levels of the different SSS estimates (model and data) but the number of match-ups between Argo, the model and the SSS data would be very limited and little spatial/temporal information would be available. This method also assumes the three estimates have uncorrelated errors which is not necessarily true: the model assimilates in situ measurements so their errors are likely to be correlated; the two satellite SSS measurements include representativity errors (when comparing them to model values) which are likely to be correlated; and the satellite SSS data have been calibrated using in situ data so those estimates are also likely to have correlated errors.

Instead, we use the model data as a reference in assessing the various satellite data-sets with a prior understanding of the errors in the model provided by Argo-model comparisons, i.e. we assume the Argo errors to be much smaller than model forecast or satellite SSS errors. In the results that follow, we first discuss Argo-model comparisons where the Argo data are compared to the model values before they are assimilated. These therefore represent independent estimates of the SSS, although previous data from the same float will have been assimilated 10 days previously.

4. Assessment of satellite surface salinity data

Model-data comparisons have been carried out with various estimates of SSS over the regions shown in Fig 2. Case study regions in the Gulf Stream and Agulhas are included in order to understand the characteristics of the salinity data in these important boundary current regions. The global region is included so that a complete picture of SSS accuracy can be obtained, and a region which excludes the high latitudes (>40° latitude) from the global statistics (called 'MidLowLats' here) is also included to understand the characteristics of the data in regions where the satellite data is expected to have improved performance (i.e. sensitivity of satellite measured brightness temperatures to salinity is higher in warmer waters). The SPURS region in the North Atlantic is included in order to understand the characteristics of the data in a region which has been well sampled by in situ data and which is less affected by land contamination or RFI.

© Crown copyright 2015

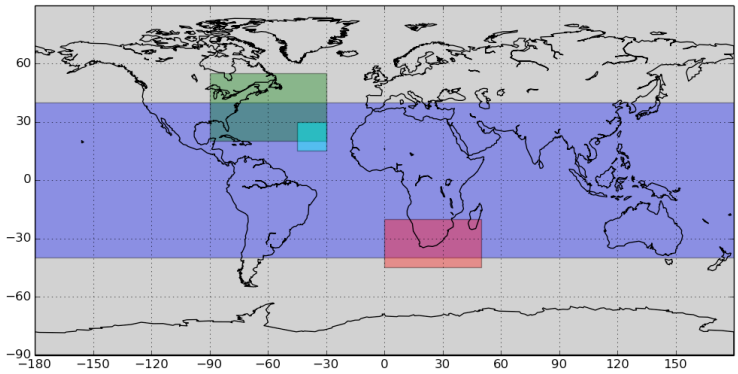

Fig 2: Validation regions. Gray: 'Global'; blue: 'MidLowLats'; green: 'GulfStream'; cyan: 'SPURS'; red: 'Agulhas'.

4.1 FOAM vs Argo

Mean and RMS differences between FOAM and Argo SSS measurements over the top 10m are shown in Fig 3 for a one year period. The biases are generally smaller than ±0.1 pss but are larger in some regions such as the Antarctic Circumpolar Current and are as large as 0.5 pss in the Gulf Stream extension region. In that region there is a dipole in the SSS mean errors with the model being too fresh to the south of the Gulf Stream front, and too salty to the north. The RMS differences are smaller than 0.2 pss over most of the ocean, but larger differences occur in the Tropical Atlantic, Eastern Tropical Pacific, Antarctic Circumpolar Current, Bay of Bengal, and the Gulf Stream regions, all areas expected to have high variability in SSS due to internal ocean dynamics, increased variability in surface precipitation and evaporation, and increased variability in river run-off.

The seasonal cycle of the mean and standard deviation of the differences are shown in Fig 4 for the regions shown in Fig 2. The model is generally biased fresh compared to the Argo measurements over the top 10m with a magnitude of up to about 0.09 pss, although most of the time, and for most regions, the bias is smaller than 0.05 pss. The global region has the largest biases, while the region between ±40° latitude has much smaller bias, indicating that the high latitudes have larger errors, particularly near the sea-ice edge (ref Fig 3). The standard deviation differences in the Gulf Stream, as well as being the highest on average, also have large month-to-month variability. Other regions tend to have fairly stable standard deviations throughout the year, with the SPURS region having the smallest random errors.

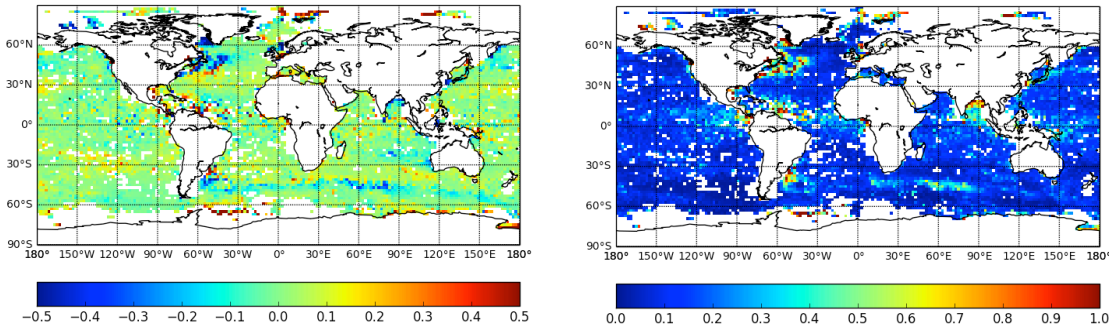

Fig 3: Argo-FOAM differences (pss) in the top 10m of the ocean calculated over the period 1st Dec 2011 to 30th Nov 2012 in 2°x2° bins: (a) mean differences and (b) root-mean-square differences.

© Crown copyright 2015

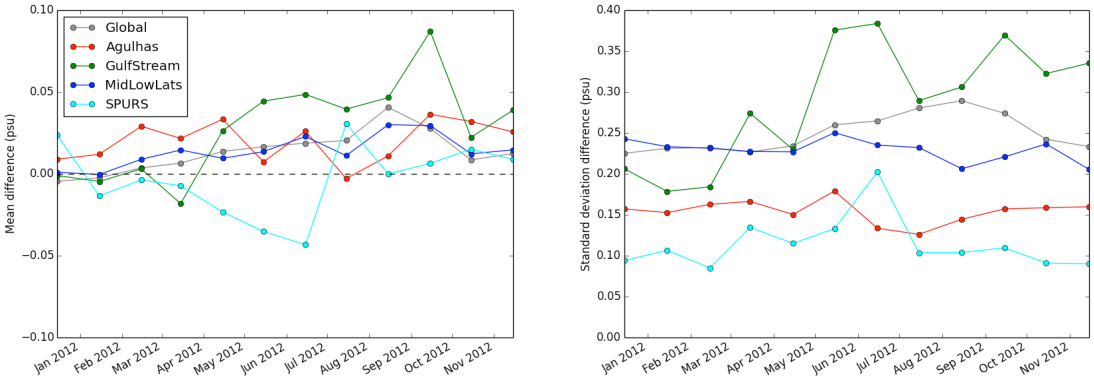

Fig 4: Monthly time-series of the (a) mean and (b) standard deviation of the differences between FOAM and Argo observations (Argo-FOAM) for observations in the top 10m, in various ocean regions.

4.2 Which SMOS product to use?

Taylor plots (Taylor 2001) are used in this section to summarise some of the statistics of the data. On these plots, the correlation coefficient is shown as the angle from the y-axis (the correlation coefficient values are shown on the arc between the top of the y-axis and the x-axis). The distance from the (0.,0.) point indicates the ratio of the standard deviation of the data to the standard deviation of the equivalent model values with a value of one shown as the dashed line; a dot which is closer to (0.,0.) than this line indicates that the observations have less variability than the model. The third quantity which is shown on this plot is the normalised centred root-mean-square difference (normalised CRMSD) between the observations and the model. The grey solid lines show values of equal normalised CRMSD which is calculated by removing the mean model value from the model, and the mean observation value from the observations, and calculating the RMS of the differences between these centred model and observation values. The resulting CRMSD is then normalised by the standard deviation of the model values, so that a value of 1.0 implies that the CRMSD is the same as the variability in the model, while a value of much less than 1.0 implies that the observations and model agree with each other much more closely than the underlying variability of the model. The fact that the values are calculated as centred values means that any biases between the model and the observations will not be reflected in these plots.

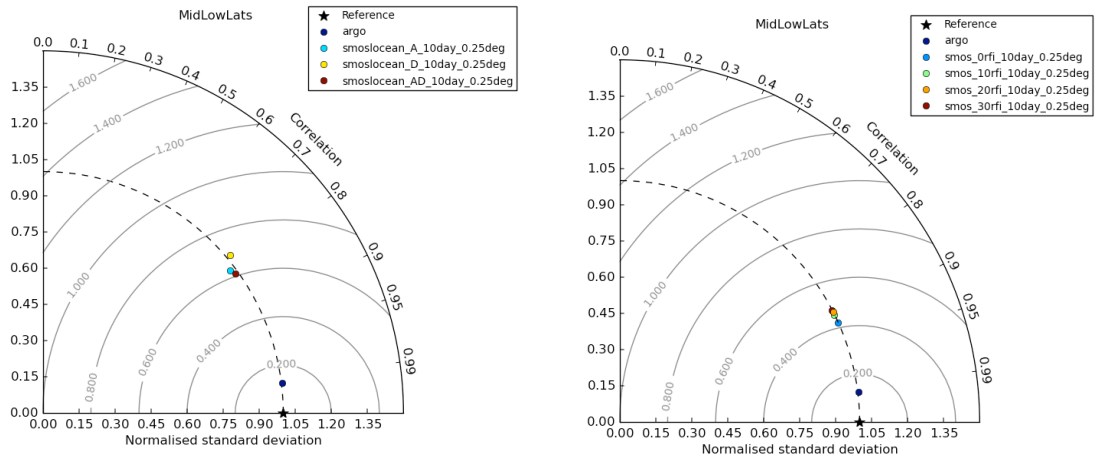

Fig 5. Taylor plots for the MidLowLats region showing the normalised standard deviation, normalised CRMSD and correlation coefficient for FOAM-Argo and FOAM-

© Crown copyright 2015

SMOS collocations over the full year 1st Dec 2011 to 30th Nov 2012. (a) shows the impact of using ascending, descending or both types of data in the SMOS processing of LOCEAN, (b) shows the impact of using different levels for the probability of RFI contamination in the Ifremer data.

4.2.1. Ascending vs descending SMOS data

Figure 5(a) shows a Taylor plot comparing the SMOS data from LOCEAN and FOAM data calculated over the MidLowLats region (all data within ±40° latitude). Comparisons of the 10 day averaged data with 1/4° horizontal resolution have been made with the equivalent FOAM data for one year, and statistics of the differences calculated. This has been done with three different versions of the data: data from ascending passes only; data from descending passes only; and data based on both ascending and descending passes. For comparison, statistics of the instantaneous Argo-FOAM differences are also shown on this and subsequent plots. This plot confirms the conclusions from previous studies that the descending SMOS data has larger random errors than the ascending SMOS data, and that the combined ascending/descending data is the most accurate.

4.2.2. RFI flags in SMOS data

Figure 5(b) shows a Taylor plot comparing the Ifremer SMOS data with FOAM over the same MidLowLats region, also with 10-day averaged data and 1/4° horizontal resolution. Here the different points on the plot show the statistics when different flags have been chosen for the probability of RFI contamination. As expected, the differences between the data and the model are smallest when only data with zero probability of RFI are chosen. When observations with 10% probability of RFI are also included, the normalised CRMSD increases and the correlation coefficient decreases. When even more data are included with higher probability of RFI (20% and 30%), there are further small degradations in the statistics. This implies that data with 0% probability of RFI should be chosen for comparisons with the model, and that the degradation in the statistics outweighs any benefits from increase in spatial coverage from including extra data.

Comparing the statistics of the ascending and descending LOCEAN data (on Fig 5(a)) with those of the 0% RFI Ifremer data (on Fig 5(b)) shows that the Ifremer data agree more closely with the FOAM data. The normalised CRMSD is roughly 50% larger in the LOCEAN data than the Ifremer data and the correlation coefficient about 0.1 smaller. These improved statistics could be due to a number of factors, including the fact that the Ifremer processing includes a correction to climatology which corrects for large-scale systematic biases in some regions/seasons (see Hernandez *et al*., 2014), and the model also relaxes the surface salinity towards climatology. For subsequent comparisons in this section, we use the SMOS data processed by Ifremer.

4.2.3. Temporal averaging

For assimilation of data into FOAM, we would ideally use daily resolution data, as the time window of the assimilation is one day. Fig 6 shows the impact on the statistics from temporally averaging the data on daily, 10 day and monthly time-scales for different regions (in each case the model is averaged in the same way as the data).

© Crown copyright 2015

As expected, the model and SMOS data agree more closely as the temporal averaging is increased. The monthly and 10-day averaged data have more similar statistics than the daily averaged data. This implies that the model and observations have more similar low frequency variability than the day-to-day variability.

Figure 7 shows the impact of temporal averaging on the RMS differences in the Gulf Stream and Agulhas regions. This shows that the daily 1° SMOS-FOAM differences are of the order of 3-10 times the instantaneous Argo-FOAM differences while the 10-day averaged SMOS-FOAM differences are more similar to the Argo-FOAM differences away from the coast. For both levels of averaging, the SMOS data agree much more closely with the model in the Gulf Stream region than in the Agulhas where land contamination seems to be a particular issue.

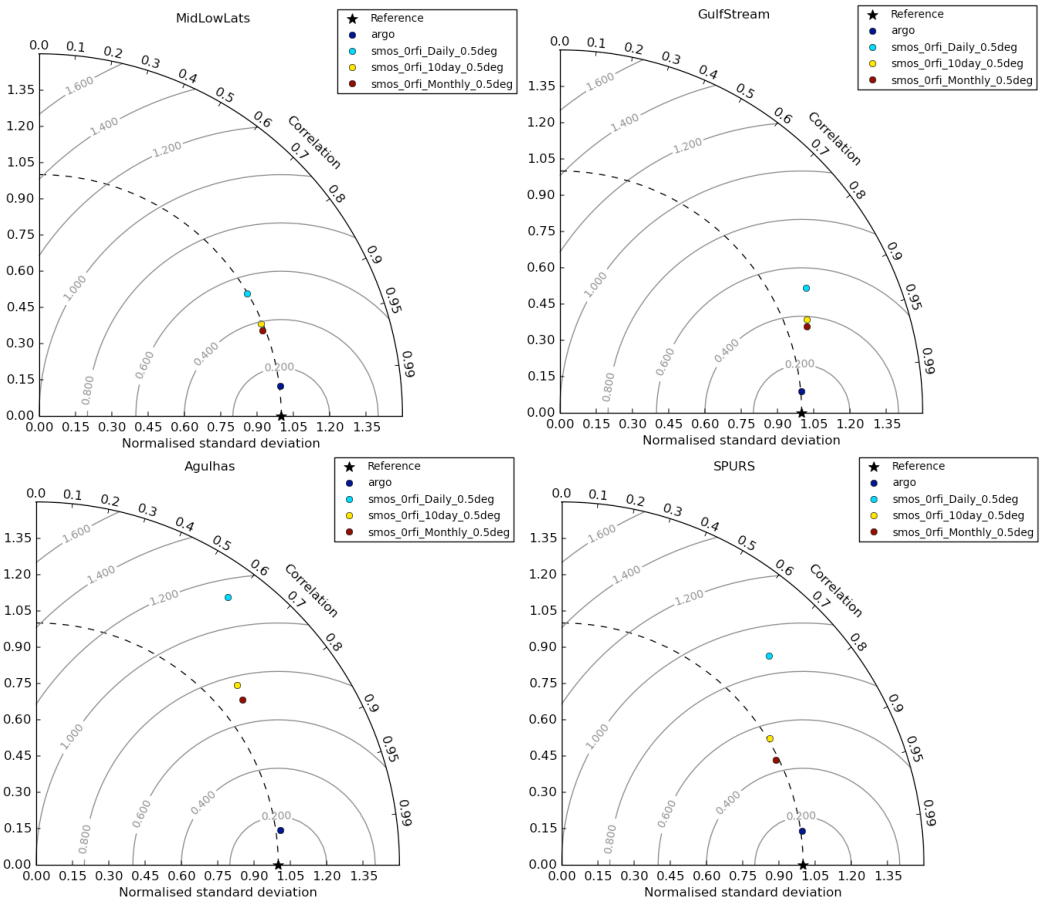

Fig 6. Taylor diagrams as described in the caption of Fig 5, showing the impact of the using daily, 10-daily and monthly averaging in the Ifremer SMOS processing, all at 0.5° resolution. The FOAM data are averaged over the same periods. (a) in the MidLowLats regions, (b) in the GulfStream region, (c) in the Agulhas region and (d) in the SPURS region.

© Crown copyright 2015

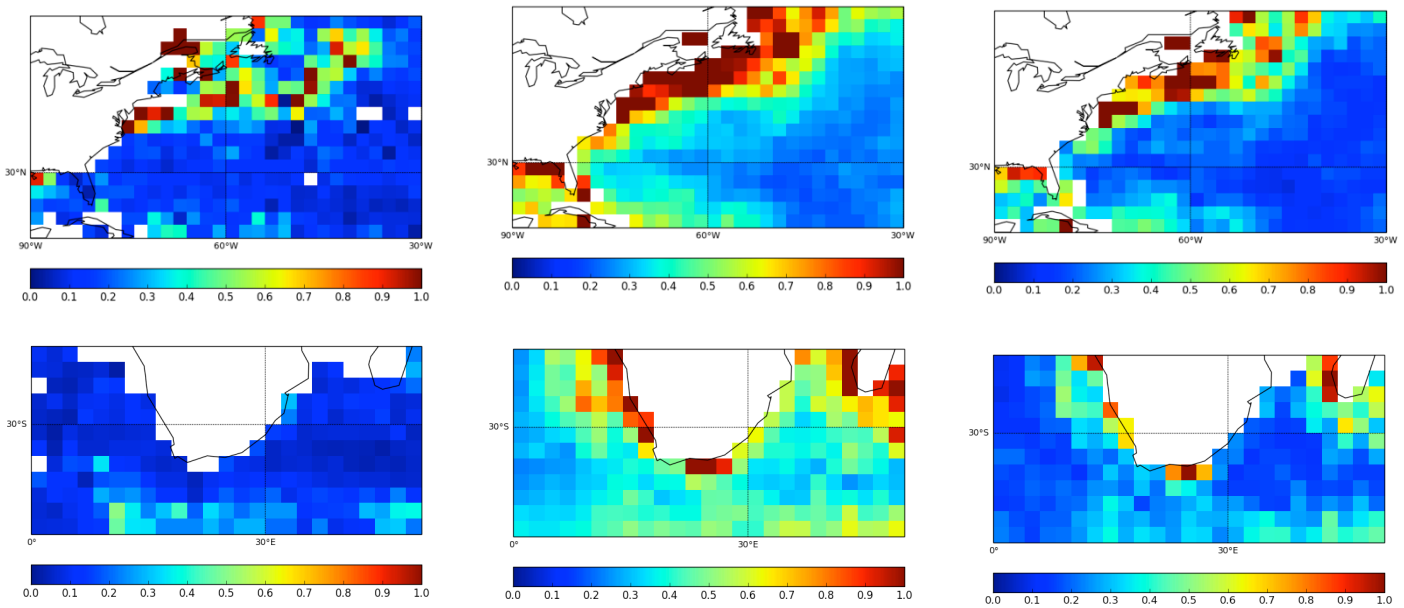

Fig 7. Impact of temporal averaging on the RMS differences between the SSS data and FOAM (pss). The top row shows the comparisons in the Gulf Stream region while the bottom row shows them in the Agulhas region. The left plots are comparisons with Argo data, the middle plots are for SMOS data with daily averaging and the right plots are for data with 10-day averaging, all with 1° horizontal resolution.

© Crown copyright 2015

4.2.4. Spatial averaging

Figure 8 shows the impact of different levels of spatial averaging, ranging from 1/4° to 1° resolution, on the SMOS-FOAM statistics in different regions, for 10-day temporally averaged data. As expected, the larger spatial averaging improves the comparison between the model and data implying that the two estimates agree more closely on larger spatial scales, whilst at scales similar to those of mesoscale features, the data do not agree so well. This is particularly evident in the Agulhas and SPURS regions.

Figure 9 shows the RMS differences in the Gulf Stream and Agulhas regions for data with different spatial averaging. The spatial averaging has a large impact in these regions with a significantly improved comparison at 1° resolution compared to 1/4° resolution. This improvement is probably due to the fact that the SMOS data has significant amount of noise at the mesoscale, whilst the model's mesoscale features may also not always be in the correction position. At 1° resolution over 10 days the SMOS-FOAM RMS differences are approximately twice the instantaneous Argo-FOAM differences, away from the coastal regions.

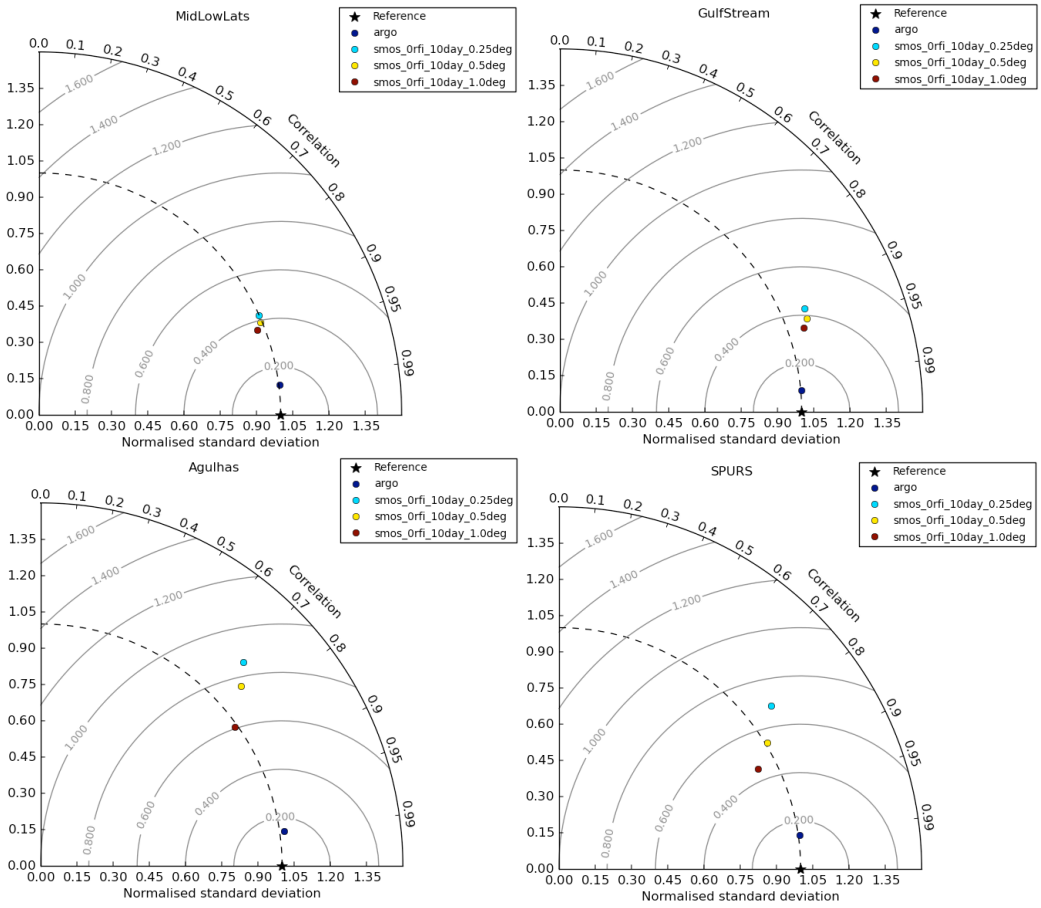

Fig 8. Taylor diagrams as described in the caption of Fig 4, showing the impact of the using 0.25°, 0.5° and 1° spatial averaging in the Ifremer SMOS processing, all calculated using the 10-day temporal averaging. The FOAM data are calculated with the equivalent spatial averaging. (a) in the MidLowLats regions, (b) in the GulfStream region, (c) in the Agulhas region and (d) in the SPURS region.

© Crown copyright 2015

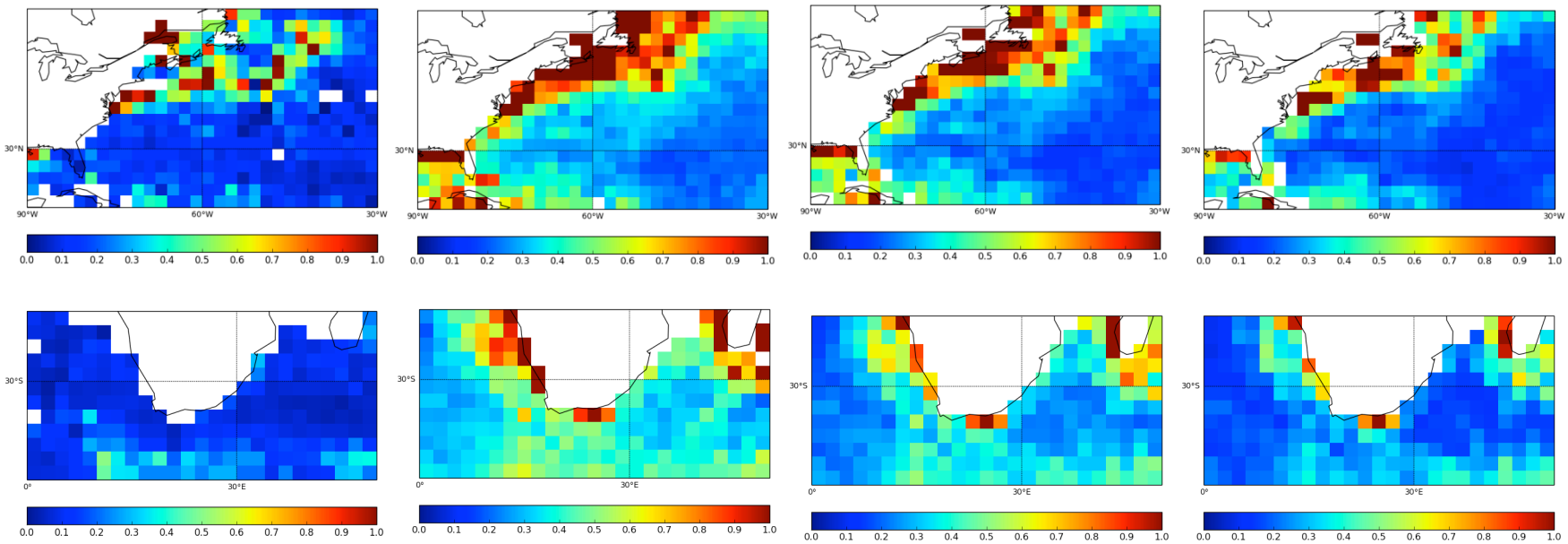

Fig 9. Impact of spatial averaging on the RMS differences between the SSS data and FOAM (pss). The top row shows the comparisons in the Gulf Stream region while the bottom row shows them in the Agulhas region. The left plots are comparisons with Argo data, the second column are for SMOS data with 1/4° averaging, the third column are for data with 1/2° averaging, and the right column are for data with 1° averaging, all with 10-day temporal averaging.

© Crown copyright 2015

4.3 Comparison of SMOS and Aquarius

The daily 1° resolution SMOS data produced by Ifremer have been used to compute global mean and RMS differences to FOAM and are shown in Fig. 10. Also shown are the Aquarius-FOAM differences with the same spatial and temporal sampling. The biases in the two satellites are significant and have rather different spatial structures. The Aquarius-FOAM differences have large (about 0.2 pss) biases at mid-latitudes in both hemispheres with smaller biases in the tropics, and they have significant negative biases (greater than 0.5 pss) at latitudes greater than about 60°. The SMOS-FOAM differences have large biases in the region of the ITCZ, particularly in the Atlantic, large negative biases around the western coasts of most of the continents, and a positive bias in mid-latitudes. At higher latitudes, the SMOS-FOAM biases are significant, but do not have such a coherent structure as the Aquarius-FOAM differences.

The RMS differences shown in Fig 10 appear to be of a similar level in the Aquarius and SMOS data over most of the globe, although the SMOS data appear to agree better with the FOAM data in most regions away from land. The SMOS data are closer to the model values in most of the ocean basins, and particularly at high latitudes, although the two satellites show similar differences in the tropics. The Aquarius data are closer to the model values around the coasts, particularly in the northern Indian Ocean and the eastern Tropical Pacific.

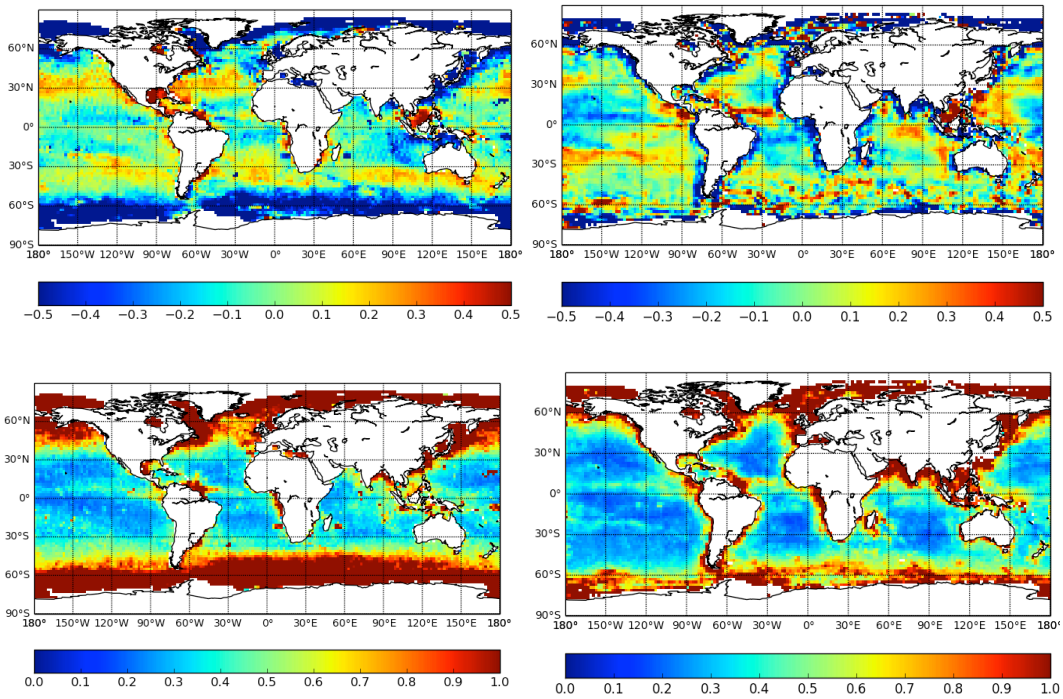

Fig 10. Top row shows the mean differences and bottom row shows the RMS differences (pss) of the FOAM-satellite data collocations in 2°x2° bins over the period 1st Dec 2011 to 30th Nov 2012. The left column shows the Aquarius daily 1° results and the right column shows the SMOS daily 1° results.

© Crown copyright 2015

5. Spatial information in SMOS

In this section we investigate whether the spatial structures in the SSS estimated by SMOS and FOAM model output agree with each other and with other data types, and whether the SMOS data contain information about spatial structures which is complementary to other datasets. In order to do this, the SMOS and model data have been averaged onto a 1/4°x1/4° grid for January 2012 and August 2012. Satellite SST data have also been averaged onto the same grid for the same months, and satellite altimeter sea surface height (SSH) data have been averaged onto 1/2°x1/2° bins. In all cases the model equivalents of the observations have been binned in the same way as the observations (i.e. the model values valid at the same time as the observations are interpolated to the observation locations before they are binned). Based on these monthly average gridded values, horizontal gradients of the fields have been calculated in both the meridional and zonal directions, and their magnitude calculated. We also compare these fields to the OSCAR current data.

Figure 11 shows the SSH gradients from the observations and the model for Jan 2012 together with the OSCAR surface current speed averaged over the same month in the Gulf Stream region. The SSH gradients in the model agree well with those of the altimeter observations and the OSCAR currents, with most of the mesoscale structures being in the same place with a similar magnitude. This gives us confidence that the model dynamics and data assimilation are placing the mesoscale structures in the correct location.

The horizontal gradients of SST are shown in Fig 12 for Jan 2012. Again model and observed gradients are very similar with two clearly defined high gradient regions near the separation of the Gulf Stream, one to the north and one to the south of the main Gulf Stream front. The SST and SSH data used in these comparisons are assimilated into the FOAM system, but these comparisons have been carried out with data before it is assimilated (comparing the observations with the model background before assimilation). The data are therefore somewhat independent, but data from similar satellites will have been assimilated on previous assimilation cycles so the comparisons are not completely independent.

Figure 13 shows the horizontal SSS gradients from the SMOS data processed by Ifremer (0% RFI data) and LOCEAN (combined ascending/descending data), and the equivalent gradients from FOAM. The gradients from the two satellite products are very different with the Ifremer product having much larger gradients and smaller scale features, part of them being possibly induced by the bias correction. In both products it is possible to discern the main Gulf Stream front but it is rather noisy and incoherent compared to the calculation from the other data types. The model gradients in SSS are more coherent and the main Gulf Stream front appears to follow the northern SST front, whilst there doesn't appear to be a high SSS gradient region to the south of the main front as there is in SST. There is some indication of this southern high gradient region in the LOCEAN SSS data although it is even more incoherent than the main high gradient region. Whether this is a real feature in SSS, or whether it is an artefact of the processing, such as coming from the use of SST data in the retrieval of SSS, is an open question.

Figure 14 shows the SSH gradients from observations and model as well as OSCAR surface currents for Aug 2012. In this month, most of the mesoscale structures are in the same place in the model as they are in the observations, but there are some eddies and meanders which are in different locations (for example the meander centred at about 68°W, 37°N). The surface warming during the summer months

© Crown copyright 2015

masks most of the underlying dynamics from the SST gradient plots in Fig 15 and so SST comparisons are not useful for diagnosing the underlying ocean circulation during these summer months (although obviously they are useful for assessing other model aspects such as the input of heat). However, the SSS gradients do still show the circulation patterns as can be seen in Fig 16. Here the SSS data from Ifremer and LOCEAN show a high gradient region in the location of the main Gulf Stream front with similar structures to those of the SSH data, particularly obvious in the LOCEAN data. This signature of the underlying circulation is not present in the model SSS gradients and may indicate that the model is not properly representing the SSS structure near the surface. This also demonstrates that the satellite SSS data is providing useful information, particularly in the summer months, which could be used to understand and correct model forecast errors.

© Crown copyright 2015

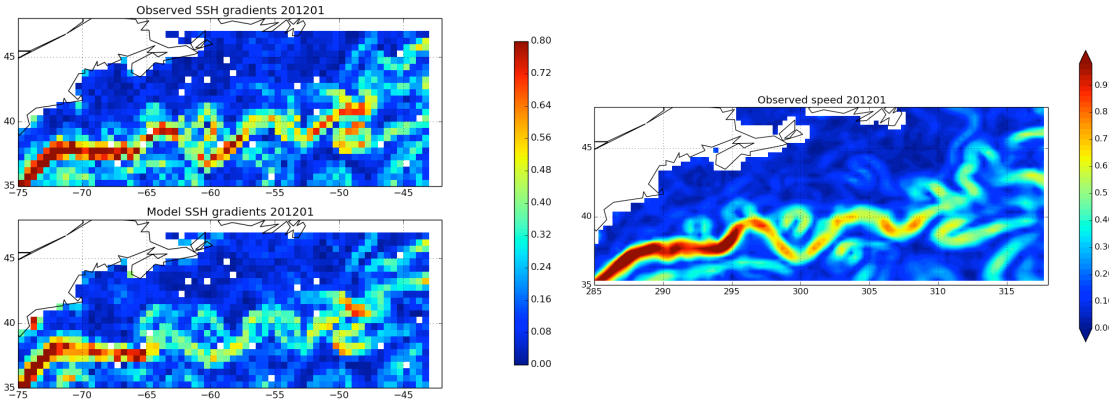

Fig 11. Horizontal gradients of sea surface height (m deg^{-1}) in 0.5°x0.5° bins for Jan 2012 in the Gulf Stream region. The top-left plot shows the observed gradients while the bottom-left plot shows the modelled gradients, calculated at the same locations as the observations. The plot on the right shows the observed near-surface current speed obtained from the OSCAR data-set.

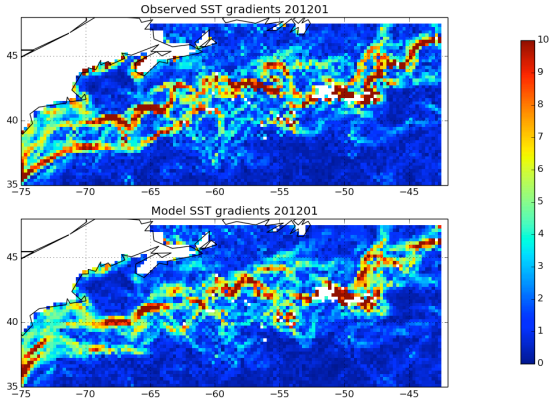

Fig 12. Horizontal gradients of SST (°C deg^{-1}) in 0.25°x0.25° bins for Jan 2012 in the Gulf Steam region. The top plot is from the observations and the bottom plot is from the equivalent model values.

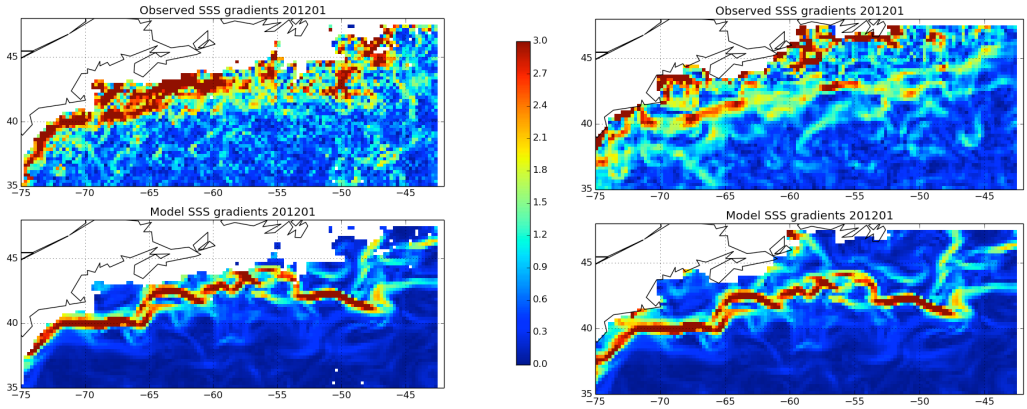

Fig 13. Horizontal gradients of SSS (pss deg^{-1}) in 0.25°x0.25° bins for Jan 2012 in the Gulf Steam region. The left column shows the gradients for the Ifremer SMOS data while the right column shows the gradients for the LOCEAN data. The top row is from the observations and the bottom row is from the equivalent model values.

© Crown copyright 2015

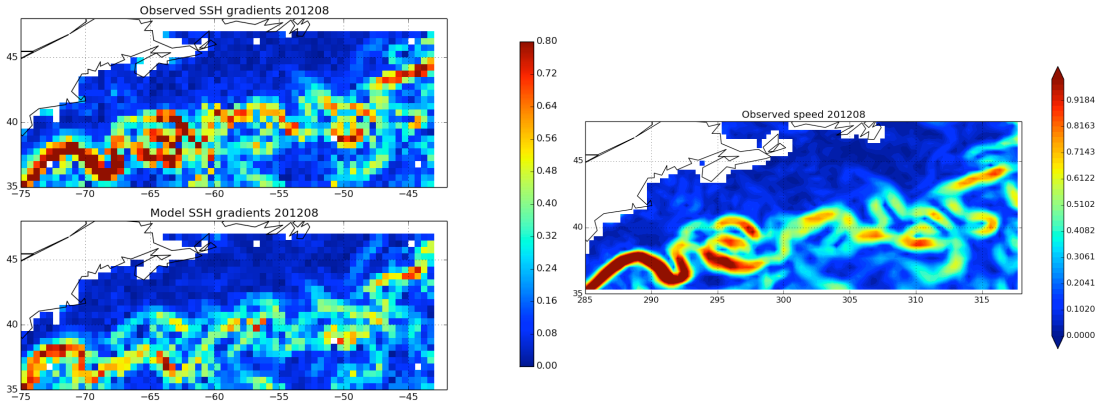

Fig 14. Horizontal gradients of sea surface height (m deg^{-1}) in 0.5°x0.5° bins for Aug 2012 in the Gulf Stream region. The top-left plot shows the observed gradients while the bottom-left plot shows the modelled gradients, calculated at the same locations as the observations. The plot on the right shows the observed near-surface current speed obtained from the OSCAR data-set.

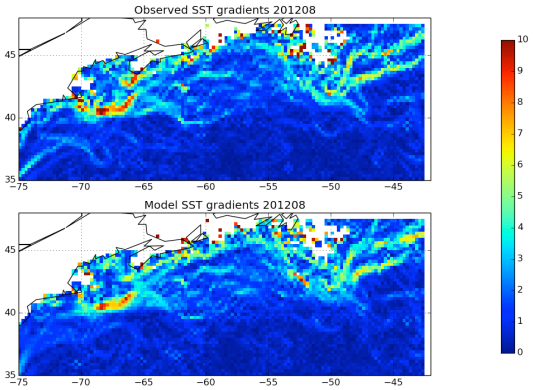

Fig 15. Horizontal gradients of SST (°C deg^{-1}) in 0.25°x0.25° bins for Aug 2012 in the Gulf Steam region. The top plot is from the observations and the bottom plot is from the equivalent model values.

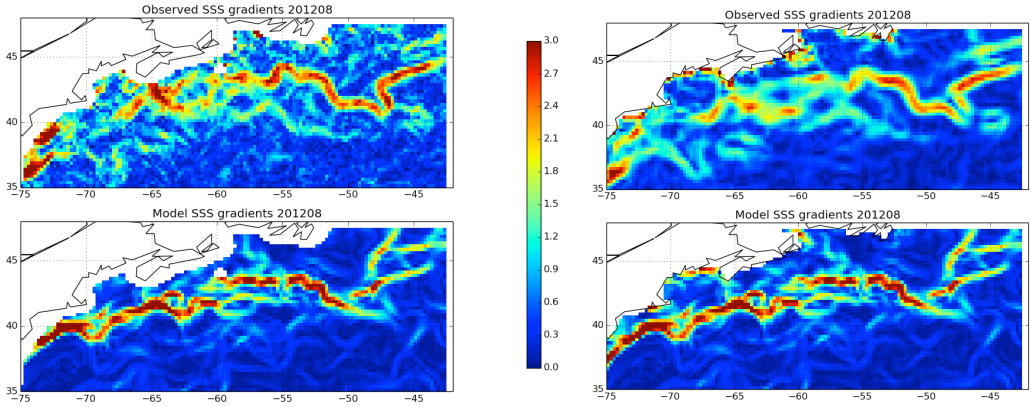

Fig 16. Horizontal gradients of SSS (pss deg^{-1}) in 0.25°x0.25° bins for Aug 2012 in the Gulf Steam region. The left column shows the gradients for the Ifremer SMOS data while the right column shows the gradients for the LOCEAN data. The top row is from the observations and the bottom row is from the equivalent model values.

© Crown copyright 2015

6. Conclusions and discussion

Comparisons of FOAM data with Argo near-surface salinity data, various versions of the SMOS satellite data, and the Aquarius satellite data, were carried out for the period Dec 2011 to Nov 2012. The Argo-FOAM comparisons showed the RMS differences are smaller than 0.2 pss over most of the ocean with the model being generally biased fresh compared to the Argo measurements over the top 10m with a magnitude for most regions of less than 0.05 pss. Comparisons of various SMOS products showed that the ascending and descending combination provides the best comparison with the model, and it is important to use data with a 0% probability of RFI. The Ifremer product agreed with the model more closely than the LOCEAN product, although it must be emphasised that the Ifremer product uses climatology in its processing and the FOAM model relaxes to climatological SSS during the forecast. The SMOS-FOAM differences were similar in magnitude to the Aquarius-FOAM differences over most of the globe, with SMOS-FOAM differences being slightly smaller in the interior of the ocean and at high latitudes while Aquarius-FOAM differences were smaller around many of the coasts.

In the Gulf Stream region in summer months the SMOS data were shown to contain spatial structures which agreed well with other satellite datasets including the altimeter SSH data and the OSCAR currents. Some of these features were not represented in the model's SSS gradients indicating an issue in the model's representation of SSS, and the features are not shown in the SST gradients during the summer months when the surface heating by the atmosphere masks the underlying circulation in the SST. The SSS data therefore contains useful information about these spatial structures which could be extracted through data assimilation techniques.

In order to assimilate SSS data from SMOS and Aquarius, a number of steps would need to be carried out. Quality control of the data will be crucial as it will be important to remove "bad" observations (e.g. those affected by RFI, land contamination, data at high latitudes, and data with other gross errors) without removing too many "good" observations, and the definition of "bad" and "good" will need to be carefully defined using statistical techniques as is done for other data types (see for example Ingleby and Huddleston, 2007). The large biases in SMOS and Aquarius data will also need to be removed before assimilation as most assimilation methods assume the observations to be unbiased. Two options to deal with the significant biases in the satellite data are: (i) remove biases prior to assimilation using techniques similar to those used for satellite SST data (see Donlon et al. 2012); or (ii) assimilate anomalies calculated relative to a long-time average of the SSS data, as is currently done for altimeter SSH data assimilation. Option (i) would be preferable as the full SSS field would then be assimilated, but it relies on there being enough "reference" SSS observations for the bias correction to work well and the current network of in situ SSS measurements is much sparser than that for SST. The issue of in situ measurements and satellite measurements being valid at different depths would also need careful consideration for this option to work well. The second option would avoid some of these problems, but has the disadvantage that the full SSS field could not be corrected by the assimilation.

Successful assimilation of the satellite SSS data also requires a good knowledge of the random component of the errors in the model and in the data. With such large errors in the data, it would be important not to under-specify the errors in the observations, otherwise we would assimilate noise. The comparisons shown in this

© Crown copyright 2015

report could provide a good basis for assigning errors in any preliminary assimilation experiments to be carried out.

Acknowledgements

This work has been carried out as part of the ESA project SMOS+SOS (see http://www.smos-sos.org/ for more information about the project). SMOS data have been provided by Ifremer and LOCEAN through the CATDS data portal (http://www.catds.fr/) and advice on their use provided by Nicolas Reul and Jacqueline Boutin. Jacqueline Boutin, Chris Banks of the National Oceanography Centre, Southampton (NOCS) and John Siddorn of the Met Office provided useful feedback on the first draft of this report.

© Crown copyright 2015

References

Blockley, E. W., Martin, M. J., McLaren, A. J., Ryan, A. G., Waters, J., Lea, D. J., Mirouze, I., Peterson, K. A., Sellar, A., and Storkey, D.: Recent development of the Met Office operational ocean forecasting system: an overview and assessment of the new Global FOAM forecasts, Geosci. Model Dev., 7, 2613-2638, doi:10.5194/gmd-7-2613-2014, 2014.

Boutin, J., N. Martin, G. Reverdin, X. Yin and F. Gaillard, Sea surface freshening inferred from SMOS and ARGO salinity: Impact of rain, Ocean Sci., 9, 183-192, doi:10.5194/os-9-183-2013, 2013

Donlon, C. & Co-Authors (2010). "Successes and Challenges for the Modern Sea Surface Temperature Observing System" in Proceedings of OceanObs'09: Sustained Ocean Observations and Information for Society (Vol. 2), Venice, Italy, 21-25 September 2009, Hall, J., Harrison, D.E. & Stammer, D., Eds., ESA Publication WPP-306, doi:10.5270/OceanObs09.cwp.24

Donlon, C.J., M. Martin, J. D. Stark, J. Roberts-Jones, and E. Fiedler, 2012. The Operational Sea Surface Temperature and Sea Ice Analysis (OSTIA) system. Rem. Sens. of Environment. 116: 140-158. http://dx.doi.org/10.1016/j.rse.2010.10.017.

Font, J., J. Boutin, N. Reul, P. Spurgeon, J. Ballabrera-Poy, A. Chuprin, C. Gabarro, J. Gourrion, S. Guimbard, C. Hénocq et al., (2012) SMOS first data analysis for sea surface salinity determination, International Journal of Remote Sensing, DOI:10.1080/01431161.2012.716541.

Freeland, H. & Co-Authors (2010). "Argo - A Decade of Progress" in Proceedings of OceanObs'09: Sustained Ocean Observations and Information for Society (Vol. 2), Venice, Italy, 21-25 September 2009, Hall, J., Harrison, D.E. & Stammer, D., Eds., ESA Publication WPP-306, doi:10.5270/OceanObs09.cwp.32

Gierach, M.M., J. Vazquez, T. Lee, and V. Tsontos, 2013: Aquarius and SMOS detect effects of an extreme Mississippi River flooding event in the Gulf of Mexico. Geophys. Res. Lett., 40, doi:10.1002/grl.50995.

Grodsky, S. A., N. Reul, G. Lagerloef, G. Reverdin, J. A. Carton, B. Chapron, Y. Quilfen, V. N. Kudryavtsev, and H.-Y. Kao (2012), Haline hurricane wake in the Amazon/Orinoco plume: AQUARIUS/SACD and SMOS observations, Geophys. Res. Lett., 39, L20603, doi:10.1029/2012GL053335.

Henocq, C., J. Boutin, G. Reverdin, F. Petitcolin, S. Arnault, and P. Lattes, 2010: Vertical Variability of Near-Surface Salinity in the Tropics: Consequences for L-Band Radiometer Calibration and Validation. J. Atmos. Oceanic Technol., 27, 192–209. http://dx.doi.org/10.1175/2009JTECHO670.1

Hernandez, O., J. Boutin, N. Kolodziejczyk, G. Reverdin, N. Martin, F. Gaillard, N. Reul, and J. L. Vergely (2014), SMOS salinity in the subtropical North Atlantic salinity maximum: 1. Comparison with Aquarius and in situ salinity, J. Geophys. Res. Oceans, 119, 8878–8896, doi:10.1002/2013JC009610.

Hunke, E. C. and Lipscomb, W. H.: CICE: the Los Alamos sea ice model. Documentation and software users manual, Version 4.1 (LA-CC-06-012), T-3 Fluid Dynamics Group, Los Alamos National Laboratory, Los Alamos, 2010. 6221, 6225.

© Crown copyright 2015

Ingleby, B., and M. Huddleston, 2007: Quality control of ocean temperature and salinity profiles - historical and real-time data. Journal of Marine Systems, 65, 158-175 10.1016/j.jmarsys.2005.11.019

Köhl, A., M. Sena Martins, and D. Stammer (2014), Impact of assimilating surface salinity from SMOS on ocean circulation estimates, J. Geophys. Res. Oceans, 119, 5449–5464, doi:10.1002/2014JC010040.

Lagerloef, G., Wentz, F., Yeuh, S., Kao, H., Johnson, G., and Lyman, J. (2012). Aquarius Satellite Mission Provides New Detailed View of Sea Surface Salinity, in State of the Climate in 2011, Bull. Amer. Meteor. Soc., 93 (7), S70-S71.

Le Vine, D.M., S. Abraham, 2004. Galactic noise and passive microwave remote sensing from space at L-band. Geoscience and Remote Sensing, IEEE Transactions, 42, 119 – 129.

Lee, T., G. Lagerloef, M.M. Gierach, H.-Y. Kao, SS. Yueh, and K. Dohan, 2012: Aquarius reveals salinity structure of tropical instability waves. Geophys. Res. Lett., 39, L12610, doi:10.1029/2012GL052232.

Madec G. 2008: "NEMO ocean engine". Note du Pole de modélisation, Institut Pierre-Simon Laplace (IPSL), France, No 27 ISSN No 1288-1619.

Oliva, R., E. Daganzo , Y. Kerr , S. Mecklenburg , S. Nieto , P. Richaume and C. Gruhier "SMOS Radio Frequency interference scenario: Status and actions taken to improve the RFI environment in the 1400–1427-MHz passive band", IEEE Geosci. Remote Sens., vol. 50, no. 5, pp.1427 -1439 2012

Reul, N., J. Tenerelli, B. Chapron and P. Waldteufel, “Modelling Sun glitter at L-band for the Sea Surface Salinity remote sensing with SMOS”, IEEE Transactions on Geoscience and Remote Sensing, vol 45, No 7, pp 2073-2087, 2007.

Reul, N., B. Chapron, T. Lee, C. Donlon, J. Boutin, and G. Alory (2014), Sea surface salinity structure of the meandering Gulf Stream revealed by SMOS sensor, Geophys. Res. Lett., 41, 3141–3148, doi:10.1002/2014GL059215.

Tang, W., S. H. Yueh, A. G. Fore, and A. Hayashi (2014), Validation of Aquarius sea surface salinity with in situ measurements from Argo floats and moored buoys, J. Geophys. Res. Oceans, 119, 6171–6189, doi:10.1002/2014JC010101.

Taylor, K. E. (2001), Summarizing multiple aspects of model performance in a single diagram, J. Geophys. Res., 106(D7), 7183–7192, doi:10.1029/2000JD900719.

Vinogradova, N. T., R. M. Ponte, I. Fukumori, and O. Wang (2014), Estimating satellite salinity errors for assimilation of Aquarius and SMOS data into climate models, J. Geophys. Res. Oceans, 119, 4732–4744, doi:10.1002/2014JC009906.

Waters, J., M. Martin, J. While, D. Lea, A. Weaver, I. Mirouze (2014). Implementing a variational data assimilation system in an operational 1/4 degree global ocean model. Accepted for publication in Q. J. R. Meteorol. Soc.

Wunsch, C., and P. Heimbach (2013), Dynamically and kinematically consistent global ocean circulation and ice state estimates, in Ocean Circulation and Climate: Observing and Modeling the Global Ocean, edited by G. Siedler, et al., pp. 553–580, Elsevier, Oxford, U. K.

© Crown copyright 2015

Yin, X., J. Boutin and P. Spurgeon (2012a), Optimization of L-band sea surface emissivity models deduced from SMOS data, IEEE Transactions on Geoscience and Remote Sensing, doi: 10.1109/TGRS.2012.2184547.

Yin, X., J. Boutin, and P. Spurgeon (2012b), First assessment of SMOS data over open ocean: part I Pacific Ocean, IEEE Transactions on Geoscience and Remote Sensing, 10.1109/TGRS.2012.2188407.

Yin, X., J. Boutin, G. Reverdin, T. Lee, S. Arnault, and N. Martin (2014), SMOS Sea Surface Salinity signals of tropical instability waves, J. Geophys. Res. Oceans, 119, 7811–7826, doi:10.1002/2014JC009960.

© Crown copyright 2015